HAL
open science

The equilibrium gap method with modeling parameters: identifiability conditions and sensitivity

Fabien Amiot, François Hild, Jean Paul Roger

To cite this version:

Fabien Amiot, François Hild, Jean Paul Roger. The equilibrium gap method with modeling parameters: identifiability conditions and sensitivity. 2008. hal-00245303

HAL Id: hal-00245303

https://hal.science/hal-00245303v1

Preprint submitted on 7 Feb 2008

HAL is a multi-disciplinary open access archive for the deposit and dissemination of scientific research documents, whether they are published or not. The documents may come from teaching and research institutions in France or abroad, or from public or private research centers.

L'archive ouverte pluridisciplinaire **HAL**, est destinée au dépôt et à la diffusion de documents scientifiques de niveau recherche, publiés ou non, émanant des établissements d'enseignement et de recherche français ou étrangers, des laboratoires publics ou privés.

The equilibrium gap method with modeling parameters: identifiability conditions and sensitivity

F. Amiot[a,b,*], F. Hild[b], J.P. Roger[a]

[a] *Laboratoire d'Optique Physique, ESPCI / CNRS-UPR A0005*

10 rue Vauquelin, F-75005 Paris, France

{amiot,roger}@optique.espci.fr

[b] *LMT-Cachan, ENS de Cachan / CNRS-UMR 8535 / Université Paris 6,*

61 avenue du Président Wilson, F-94235 Cachan Cedex, France

{amiot,hild}@lmt.ens-cachan.fr

[*] *Corresponding author :*

Fabien AMIOT

fax: +33.1.47.40.22.40

Email: amiot@lmt.ens-cachan.fr

Short running head title :

Parametrized identification with EGM

Abstract:

The use of a Nomarski shear-interferometer with a sinusoidal phase modulation and four integrating buckets allows one to obtain the displacement field of the surface of a micro-cantilever observed in reflection microscopy. One can apply an electrostatic loading to this micro-object, which is first represented as an unknown pressure field. When retrieving both the flexural stiffness field and the load field using the equilibrium gap method, one may model the applied loading as a pure pressure field. This paper intends first to assess the effect of a modeling error, and then to test the identifiability conditions if one uses a parameterized description of the loading to fit measured kinematic data. The influence of the measurement noise on the identified parameters is then semi-analytically derived, and the global identification algorithm is applied to experimental data.

Keywords: Full-field measurements / Identification problem / Inverse problem / MEMS

1. Introduction

In the last years, the decreasing cost of parallel optical acquisition systems, such as CMOS and CCD arrays, encouraged their use in mechanical engineering to perform full-field instead of pointwise (thermal or mechanical) measurements [1]. The large amount of data that is then available is used by experimentalists to check for boundary conditions in "homogeneous" tests [2] or for strain localization [3], or to deal with heterogeneous tests to validate constitutive equation parameters [4], to identify stress intensity factors [5,6,7] or elastic parameters by finite element updating [8] or the virtual fields method [9]. Full-field measurements can also be used to retrieve heterogeneous properties, by minimizing the constitutive equation error [10] or the equilibrium gap [11], or to locate cracks in a medium by using the reciprocity gap [12]. All these methods are dependent on hypotheses on the model describing the specimen under scrutiny.

The mechanical behavior of micro-electromechanical systems (MEMS) is dominated by mechanical-environment coupling phenomena because of their increased surface / volume ratio. These coupled effects are usually evaluated by using pointwise measurements, and often involve non-contact chemical loading [13]. The development of new sensors or actuators involving these new coupling phenomena requires novel modelings. Dealing with MEMS to build a coupling modeling represents then a major challenge since the geometry of the specimen as well as the techniques used to apply a mechanical loading on these microstructures are not controlled as easily as at the macroscopic scale [14]. In this context of uncertainty, using the large amount of experimental data provided by full-field measurements instead of pointwise information is thought to be the way to overcome these difficulties.

After a description of the set-up used to measure out-of-plane displacement fields, the

equilibrium gap principles are applied to identify *both* a stiffness *and* a loading field for a cantilever beam. A semi-analytical analysis is performed to study the sensitivity of both identified fields and the error estimator to a measurement noise. Since this derivation holds when the measurement noise is the only error source, controlling the noise level is a way of detecting other error sources, such as modeling errors. Then an algorithm is proposed to retrieve one additional modeling parameter, and to derive an identifiability condition and subsequent error bounds on the unknown fields and the identified modeling parameter. Last, the algorithm accuracy is assessed when using computer-generated data, and the whole identification process is applied to experimental measurements obtained on microcantilevers under an electrostatic loading.

2. Experimental measurements

The proposed identification procedure is applied in this paper to the bending of microcantilevers, so that the first step consists in building a set-up suitable for measuring the out-of-plane displacement field of reflecting objects.

2.1. Experimental set-up

The interferential microscopy imaging set-up used herein, initially proposed by Gleyzes *et al.* [15], is shown in Fig. 1. A light-emitting diode (LED, λ = 760 nm) illuminates a polarization beam-splitter. The beam reflected by the beam-splitter is polarized at 45° of the axes of a photoelastic polarization modulator. The Wollaston prism, whose axes are parallel with those of the modulator, splits the beam into two orthogonally polarized beams at a small angle between each other. These beams are focused on the sample by an objective lens. After reflection and recombination by the Wollaston prism, the beam goes through the polarization modulator and the polarization beam-splitter. The

transmitted beam is finally focused on a CCD array. The polarization beam-splitter behaves as crossed linear polarizers mounted at 45° with respect to the axes of the Wollaston prism and of the polarization modulator. The interference figure is obtained as the difference of two topographies of the surface, shifted by the Wollaston prism by a distance *d*. The distance *d* is chosen to be greater than the cantilever length. The difference between two differential topographies obtained before and after mechanical loading gives the out-of-plane displacement field. The modulation frequency is the resonance frequency of the modulator, namely 50.3 kHz.

Using a phase integration technique allows one to get the optical phase induced by the sample [16]. The optical flux collected by the pixel indexed by *(l,m)* on the CCD matrix is formally written as

$$I(l,m,t) = I_0 + A\cos\left[\phi(l,m) + \psi(t)\right]$$

where *A* is the amplitude, $\phi(l,m)$, which is to be determined, the optical phase introduced by the sample and the Wollaston prism. The phase modulation introduced by the photoelastic modulator reads

$$\psi(t) = \psi_0 \sin\left(2\pi ft + \theta\right)$$

The angles ψ_0 et θ are two parameters that can be chosen among many couples. The algorithm to obtain ϕ uses four integrating buckets, namely, if $T=1/f$ is the modulation period, four images of the interference figure can be acquired during the period *T*, so that each image results from the integration of the optical flux during a quarter of one period. One obtains four images E_p, for $p=1,2,3,4$

$$E_p = \int_{\frac{(p-1)T}{4}}^{\frac{pT}{4}} I(t)dt$$

It is the possible to determine an optimal couple (ψ_0, θ) that allows one to obtain the

phase ϕ from linear combinations of the four images

$$\tan\left[\phi\left(l,m\right)\right] = \frac{E_1 - E_2 - E_3 + E_4}{E_1 - E_2 + E_3 - E_4}$$

By assuming that the measured phase map is the consequence of the topography of the surface of interest, out-of-plane displacement fields are obtained by computing the difference $\Delta\phi_{KA}(l,m)$ between the projection (in a least-squares sense) onto a kinematically admissible basis of the measured phase map $\phi(l,m)$ at different load levels. Then, the displacement field Δz reads (in air with a refractive index equal to 1)

$$\Delta z = \frac{\lambda}{4\pi}\Delta\phi_{KA}$$

If one neglects quantification effects, the signal recorded by each pixel E_{mes} is subjected to amplitude fluctuations ΔE_{mes} due to the erratic flux of photons impinging on the pixel. These fluctuations are modeled by Poisson's law (see for instance [17])

$$\Delta E_{mes} \propto \sqrt{N}$$

where N is the number of photons impinging on a pixel. If one assumes that the behavior of the array is linear,

$$E_{mes} \propto N$$

so that the phase measurement is subjected to fluctuations depending on the number of photons used to build the interference figure

$$\frac{\Delta E_{mes}}{E_{mes}} \propto \frac{\sqrt{N}}{N}$$

As proven in Fig. 2, this interferometer is shot-noise limited. The dots are for the measured reproducibility, and the solid line is for the shot noise limitation. The achieved reproducibility is 15 pm. Sub-nanometric displacements are then resolved, and

the noise level is controlled by the number of accumulated images. Moreover, the noise is spatially uncorrelated and follows a Gaussian distribution as shown in Fig. 3. Figure 3a shows the experimental phase noise probability density, and the solid line for its fit by a zero-mean Gaussian distribution. The standard deviation is related to the number accumulated images, and is almost 2 mrad for a 1 s exposure. Figure 3b displays the autocorrelation function of a typical noise realization. This function is nearly a Dirac, thereby proving that the experimental noise is spatially uncorrelated.

2.2. Electrostatic loading set-up

An electrostatic pressure is applied, using the fact that the present MEMS is covered by a conducting gold layer, which can be utilized as an armature of a capacitor. The other armature is a stamped aluminum sheet put above the cantilever (see Fig. 4). However, the used capacitor does not lead to a homogeneous electric field between the armatures since the upper one has a hole, and the lower one has many edges. Consequently, one cannot make any assumption concerning the homogeneity of the applied pressure field.

3. Equilibrium gap minimization

The identification problem consists in recovering an elastic contrast field and a pressure contrast by using full-field kinematic measurements. Since only kinematic fields are involved, one cannot expect to recover an absolut stiffness and a loading field but only contrasts. In the present case, a cantilever beam is considered. Let us model it as a heterogeneous Euler-Bernoulli beam discretized with N elements. The elastic property field is assumed to be heterogeneous, and is modeled as a (multiplicative) contrast field C, where EIC_n is the flexural stiffness of the element n, $n \in \{ 1 \ldots N_{el} \}$. This element is also subjected to a homogeneous pressure, which is modeled by nodal forces F and bending couples B where F_m (resp. B_m) is the force (resp. couple) applied to node m, m

$\in \{ 1 \ldots N_n \}$ (see Fig. 5).

When the pressure and the stiffness field are known, the direct (classical) problem consists in finding the nodal displacement field $U=(v,\theta)$. The present analysis aims at solving the identification (inverse) problem, *i.e.* when the nodal displacement field is known (since it is measured), to find the stiffness and load fields. The element length is l. Following the equilibrium gap method [8], the equilibrium of each node is written as the stationarity of the potential energy

$$E_{pot} = \frac{EI}{2}\sum_{n=1}^{N_{el}} C_n f\left(v_{n-1}, v_n, \theta_{n-1}, \theta_n\right) - \sum_{m=1}^{N_n}\left(F_m v_m + B_m \theta_m\right)$$

where f is based on the assumed shape functions (see Appendix A). It follows, for the i-th node (adjacent to the n-th and the $(n+1)$-th elements), that

$$\frac{\partial E_{pot_{n,n+1}}}{\partial v_i} = \frac{EI}{2}\left[C_n g^- + C_{n+1} g^+\right] - F_i\left(p_n, p_{n+1}\right) = 0$$
$$\frac{\partial E_{pot_{n,n+1}}}{\partial \theta_i} = \frac{EI}{2}\left[C_n h^- + C_{n+1} h^+\right] - B_i\left(p_n, p_{n+1}\right) = 0$$

where v and θ are the components of the measured nodal displacement field U_m. The functions g^-, g^+, h^- and h^+ are derived from f. In the present case, the pressure field p is unknown, in addition to the contrast C. The equilibrium conditions give $2(N+1)$ equations with $2(N+1)$ unknowns, without any assumed boundary condition. These equations can be rewritten as

$$M\Lambda = 0$$

with the unknown vector

$$\Lambda^t = \left[C_1, p_1, \ldots, C_{N_n}, p_{N_n}\right]$$

where M is a matrix that depends only on the measured nodal fields, which can be projected onto a kinematically admissible basis, on the assumed loading pattern and on the length of the element. Since the problem is solved in the small perturbations

framework, the behavior of the structure is assumed to be linear. Using the definition of the singular value decomposition of M

$$M = HJK^t$$

where J is a diagonal matrix, H and K are orthogonal matrices, the non-trivial solution Λ is the right singular vector associated with the least singular value of M, which should be approximately equal to 0, within the machine precision. The solution is then the column of K (*i.e.* the right singular vector) corresponding to the least singular value [18]. The mechanical load and the elastic property fields are identified up to a multiplicative constant, since only kinematic data are considered. The results will thus be referred to as load and elastic property contrasts.

4. Sensitivity study

By using the results developed in Ref.[19], one can compute the Jacobian of the singular value decomposition described above with respect to any parameter. One may be first interested in computing the Jacobian of the K matrix with respect to the displacement field. This calculation is semi-analytical since it involves solving a large number of linear systems, and returns a Jacobian J_K that can be analyzed. A more detailed analysis would exhibit a single non-singular direction of unit vector U_p so that

$$J_K U_p \neq 0$$

Therefore, when the measured displacement field is subjected to a kinematically admissible measurement noise δU, the error on the identified fields depends only on the scalar value of $\delta U^t \cdot U_p$. Performing a singular value decomposition (SVD) of J_K

$$J_K = R_K S_K T_K^t$$

where the singular values are sorted in decreasing order provides U_p as the first column

of T

$$U_{p_i} = T_{K_{i1}}$$

and

$$\frac{\partial \Lambda_i}{\partial \left(\delta U^t U_p \right)} = S_{K_{11}} R_{K_{i1}}$$

By using the experimental characterization carried out in Section 1, the noise corrupting the measured field is modeled as an uncorrelated Gaussian white noise b (variance σ^2). One has to get the resulting root-mean-square error on the identified fields $\delta\Lambda^t.\Delta\Lambda$. According to the definition of an SVD, the columns of T_K are an orthonormal basis for the displacement fields, so that one can write $\delta U = \kappa\, U_p + W\, s$, where W is the matrix obtained by concatenating the columns of T_K that are orthogonal to U_p. The projection of b onto a kinematically admissible basis reads

$$\min_{\delta U} \left[\left(M_b \delta U - b \right)^t \left(M_b \delta U - b \right) \right]$$

and yields

$$A\kappa = U_p^t \left(M_b^t b - \Xi\, W \Delta^{-1} W^t M_b^t \right)$$

with the definitions

$$\begin{aligned} A &= U_p^t \left(\Xi - \Xi\, W \Delta^{-1} W^t \Xi \right) U_p \\ \Delta &= W^t \Xi^t W \\ \Xi &= M_b^t M_b \end{aligned}$$

Moreover, the displacement partition yields, using the orthogonality conditions

$$\delta U^t \delta U = B\kappa^2 - \frac{2}{A} b^t M_b F M_b^t b$$

by assuming

$$B = 1 + U_p^t \Xi\, \Theta\, \Xi\, U_p$$
$$\Theta = W \Delta^{-1} W^t W \Delta^{-1} W^t$$
$$F = \left(U_p U_p^t - W \Delta^{-1} W^t \Xi\, U_p U_p^t \right) \Xi\, \Theta + \Theta$$

Then,

$$E\left[\kappa^2 \right] = \frac{\sigma^2}{B} \left(\Xi^{-1} \Xi^{-1} + \frac{2}{A} F \right) : \Xi$$

so that

$$E\left[\delta\Lambda^t \delta\Lambda \right] = S_{K_{11}}^2 E\left[\kappa^2 \right]$$

The variance of the identified fields grows proportionally to σ^2. To assess the identification quality, one may use the equilibrium gap F_r as an error indicator

$$F_r = \delta \left(M\Lambda \right) = \delta M\Lambda + M\delta\Lambda = K_G \delta U + M\delta\Lambda$$

where K_G is the stiffness matrix of the structure. Using the previous analysis, $E[F_r^t \,.\, F_r]$ grows as $E[\kappa^2]$ and σ^2, so that when the only error source is a measurement noise, the projection error, the identification error and the equilibrium gap are proportional to each other. Previous studies [20,11] focused on the definition of a scalar global indicator, as w_r, defined by

$$w_r = \frac{\sum_i \left| F_r(i) U_{m\pm}(i) \right|}{E_s}$$

where $U_{m\pm}$ is the measured displacement field from which the rigid body motion of the two considered elements has been removed, E_s is the elastic energy of the structure. It has been shown that this indicator can assess the noise level when the assumed model is correct. It is straightforward to show from the previous development that the w_r indicator grows propotionally to σ^2, so that the w_r value is a measure of the noise level if the assumed model is suitable. For a 2-element discretization with a 1% noise/signal

ratio, the w_r value lies in the 10^{-2} range [20].

5. Retrieving a modeling parameter

5.1. Identification assuming no modeling error

The unknowns of the identification problem are the multiplicative elastic contrast and the pressure applied to each element, which is assumed to be constant along the element (see Fig. 5). The displacement field is obtained with the set-up described in Section 1 under conditions that ensure a reproducibility of almost 100 pm, and is displayed in Fig. 9a. Since the noise/signal ratio is of the order of one percent, one would expect a value of w_r in the 10^{-2} range provided the used model is suitable. Figure 9b shows the identified fields when assuming that the cantilever is subjected only to a pressure field. One can note a repulsive pressure near the clamped part of the cantilever, and the value of w_r reaches *2.8*, thereby proving the poor quality of the identification results. Since w_r is significantly different from the expected value, one can assume a modeling error. When looking at the measured displacement field in Fig. 9a, one can note a change in the cantilever curvature near its free end. Therefore, the edge effects are not fully described with the chosen modeling, and this should be modified.

5.2. Effect of a modeling error

Let us deal with the simple case of an additional unknown nodal couple M_S acting on the free end of the cantilever. It is described by a single degree of freedom using the parameter

$$\beta = \frac{M_S}{M_{ref}}$$

Following the same procedure as in Section 2, the equilibrium gap has an additional contribution due to a modeling error

$$F_r = F_{ru} + F_{rm}$$

where F_{ru} denotes the residual due to the noise on measured fields, and F_{rm} is the residual corresponding to the modeling error. When dealing with a single modeling parameter, one can plot a 2-D map of the norm of the equilibrium gap versus $\beta - \beta_{sol}$ and $\delta U^t \cdot U_p$. Such a map, obtained with noisy computer-generated displacement fields, is shown in Fig. 6.

One can note a steep and narrow valley, which corresponds to a zero-gradient direction in the (β,$\delta U^t \cdot U_p$) plane. Let us denote by λ this zero-gradient direction, and by $\lambda_\perp$ the orthogonal one. Then, using the static criterion $\|F_r\|=0$ restricts the solution subspace to a line, whose direction is λ, thereby proving that a static criterion is not sufficient to find a solution for β.

To achieve this goal, one can note that moving to the solution is also recovering the projection onto a kinematically admissible basis of the measurement noise. By extending the analysis carried out in Section 3 to the second moment of the distribution of κ^2 leads to an additional probabilistic kinematic criterion, which is plotted in Fig. 7a, proving its complementarity to the equilibrium gap, and yielding a probability density function for given points along the λ axis. The use of this kinematic criterion allows one to restrict the solution subspace to a part of the λ axis.

5.3. Identifiability condition and identification procedure

From the previous analysis, one can locate a region in the (β,$\delta U^t \cdot U_p$) plane when combining the static criterion $\|F_r\|=0$, which sets the position along the $\lambda_\perp$ direction, and the computed probability density that defines a likely region on the λ axis. A β value can be specified if the two criteria are complementary, that is if the λ direction is not orthogonal to the $\delta U^t \cdot U_p$ direction. Since the λ direction is defined such that

$$\delta F_r = \frac{\partial F_r}{\partial U}\delta U + \frac{\partial F_r}{\partial \beta}\delta\beta = 0$$

this condition reduces to

$$\left\| \frac{\partial F_r}{\partial \beta} \right\| \neq 0$$

which is automatically satisfied if the modeling error introduces an additional contribution to the equilibrium gap. Last, one gets a probability density for the parameter β (see Fig. 7b), which may be integrated to give error bounds. This last probability density is obtained by a rescaling of the probability density of κ by using a ratio r expressed as

$$r = \frac{\left\| \frac{\partial F_r}{\partial U} \right\|}{\left\| \frac{\partial F_r}{\partial \beta} \right\|}$$

thus defining the identification sensitivity of the modeling parameter.

5.4. Retrieving a modeling parameter and identified fields

A way of improving the modeling used in Section 4.1 is to consider that the electrostatic pressure applies on all the metallic faces of the cantilever, so that the pressure on the end surface will lead to an extra couple M_S acting on the end of the cantilever (see Fig. 8). This extra couple is modeled by a dimensionless parameter β, which is the ratio between the nodal couple due to the pressure field arising on the last element M_{ref} and this extra couple M_S. With standard cubic interpolating functions, M_{ref} is given by

$$M_{ref} = -p_{N_{el}} \frac{l}{12}$$

To identify the unknown value β, one uses a relaxation algorithm:

•find a rough estimate β_0, as the minimizer of $||F_{rm}||$ with respect to β, using the

measured displacement field,

•use the computed Jacobian and a Newton-Raphson algorithm, move down the valley of the static criterion,

•define the λ direction, and compute the probability density arising from the kinematic criterion along it. Project the region of interest onto the β axis and get a probability density function for β.

For this case, the r ratio is computed, and $r = 4.5$. Figure 9d shows the final probability density for β. When integrating it, one is able to show for example that $P[-1.53 < \beta < -1.38]=0.9$. By choosing a particular point in the previous range, one can get new identified fields, which are displayed in Fig. 9c. These fields do not vary significantly in the considered β range. The pressure field is attractive everywhere along the cantilever, which is consistent with the identified field. Moreover, the w_r value lies in the 10^{-2} range throughout the whole β range, as expected from the sensitivity study performed in Ref. [20].

6. Conclusion

The use of an imaging interferometric set-up is proposed to retrieve out-of-plane displacement fields of MEMS cantilevers. One uses a phase integration technique, so that the measurement is shot-noise limited and the reproducibility is controlled by the number of accumulated images (*i.e.* the integration time), up to reach an optimal reproducibility in the 10 pm range. The noise corrupting the measured fields is shown to be described by a Gaussian distribution, without any spatial correlation.

After introducing the basis of the equilibrium gap method, the effects of a measurement noise on the identified fields were semi-analytically assessed, thereby proving the close relationship between the noise level on displacement measurement and different static

criteria used to assess the identification quality when the model used to describe the structure and the external loading is suitable.

The knowledge of the noise level, when compared to the static criterion, may be sufficient to detect a modeling error. An identifiability condition and a modeling parameter sensitivity index are then defined, together with a relaxation algorithm, to retrieve a single modeling parameter and bounds on the identified fields.

This technique was applied when using experimental data, obtained on a micro-cantilever subjected to an electrostatic loading. The poor description of sharp-tip effects is detected, and, since the identifiability condition is satisfied, an extra modeling parameter is recovered from the statistical description of the noise corrupting the measured field.

References

[1] Rastogi, P.K. (Edt.) (2000) *Photomechanics*. Springer, Berlin (Germany).

[2] Chevalier, L., Calloch, S., Hild, F., Marco, Y. (2001) Digital Image Correlation used to Analyze the Multiaxial Behavior of Rubber-Like Materials. *Eur. J. Mech. A/Solids* 20, 169-187.

[3] Desrues, J., Lanier, J., Stutz, P. (1985) Localization of the Deformation in Tests on Sand Samples. *Eng. Fract. Mech.* 21 (4), 251-262.

[4] Périé, J.N., Calloch, S., Cluzel, C., Hild, F. (2002) Analysis of a Multiaxial Test on a C/C Composite by Using Digital Image Correlation and a Damage Model. *Exp. Mech.* 42 (3), 318-328.

[5] McNeill, S.R., Peters, W.H., Sutton, M.A. (1987) Estimation of stress intensity factor by digital image correlation. *Eng. Fract. Mech.* 28 (1), 101-112.

[6] Forquin, P., Rota, L., Charles, Y., Hild, F. (2004) A Method to Determine the Toughness Scatter of Brittle Materials. *Int. J. Fract.* 125 (1), 171-187.

[7] Réthoré, J., Gravouil, A., Morestin, F., Combescure, A. (2005) Estimation of mixed-mode stress intensity factors using digital image correlation and an interaction integral. *Int. J. Fract.* 132, 65-79.

[8] Kavanagh, K.T. (1971) Finite Element Applications in the Characterization of Elastic Solids. *Int. J. Solids Struct.* 7, 11-23.

[9] Grédiac, M. (1989) Principe des travaux virtuels et identification. *C. R. Acad Sci. Paris* 309 (Série II), 1-5.

[10] Geymonat, G., Hild, F., Pagano, S. (2002) Identification of elastic parameters by displacement field measurement. *C. R. Mecanique* 330, 403-408.

[11] Claire, D., Hild, F., Roux, S. (2004) A finite element formulation to identify damage fields: The equilibrium gap method. *Int. J. Num. Meth. Engng.* 61 (2), 189-208.

[12] Andrieux, S., Abda, A.B., Bui, H.D. (1999) Reciprocity Principle and Crack Identification. *Inverse Problems* 15, 59-65.

[13] Lavrik, N.V., Sepaniak, M.J., Datskos, P.G. (2004) Cantilever transducers as a platform for chemical and biological sensors. *Review of Scientific Instruments* 75 (7), 2229-2253.

[14] Sharpe Jr., W.N. (2001) Mechanical properties of MEMS materials. In *Mems Handbook*, CRC Press.

[15] Gleyzes, P., Boccara, A.C., Saint-Jalmes, H. (1997) Multichannel Nomarski microscope with polarization modulation: performance and applications. *Optics Letters* 22 (20), 1529-1531.

[16] Dubois, A. (2001) Phase-map measurements by interferometry with sinuoidal phase modulation and four integrating buckets. *J. Opt. Soc. Am.* A 18, 1972-1979.

[17] Gabor, D. (1975) The transmission of information by coherent light. I. Classical theory. *J. Phys. E: Sci. Instrum.* 8, 73-78.

[18] Press, W.H., Teukolsky, S.A., Vetterling, W.T., Flannery, B.P. (1992) *Numerical Recipes in C*. Cambridge University Press, Cambridge (UK).

[19] Mathai, A.M. (1997) *Jacobians of matrix transformations and functions of matrix argument*. World Scientific Publishers.

[20] Amiot, F., Hild, F., Roger, J.P. (2004) Measuring the displacement field of microcantilevers under electrostatic loading to identify their mechanical properties. Proc. *SEM X*, SEM, 6p.

Appendix A

The function f is based on standard Hermite cubic polynomials

$$f(v_{n-1}, v_n, \theta_{n-1}, \theta_n) = \frac{12}{l^3}\left(v_n - v_{n-1}\right)^2 + \frac{4}{l}\left(\theta_n^2 + \theta_{n-1}^2 + \theta_{n-1}\theta_n\right) + \frac{12}{l^2}\left(v_{n-1}\theta_{n-1} + v_{n-1}\theta_n - v_n\theta_{n-1} - v_n\theta_n\right)$$

where l is the element length. The functions g^-, g^+, h^- and h^+ are then derived from f

$$g^-(v_{i-1}, v_i, \theta_{i-1}, \theta_i) = \frac{24}{l^3}\left(v_i - v_{i-1}\right) - \frac{12}{l^2}\left(\theta_{i-1} + \theta_i\right)$$

$$g^+(v_{i+1}, v_i, \theta_{i+1}, \theta_i) = \frac{24}{l^3}\left(v_i - v_{i+1}\right) + \frac{12}{l^2}\left(\theta_1 + \theta_{i+1}\right)$$

$$h^-(v_{i-1}, v_i, \theta_{i-1}, \theta_i) = \frac{12}{l^2}\left(v_{i-1} - v_i\right) + \frac{4}{l}\left(\theta_{i-1} + 2\theta_i\right)$$

$$h^+(v_{i+1}, v_i, \theta_{i+1}, \theta_i) = \frac{12}{l^2}\left(v_i - v_{i+1}\right) + \frac{4}{l}\left(\theta_{i+1} + 2\theta_i\right)$$

The functions g^- and g^+ correspond to the contributions of two adjacent elements (of a given node i) to the equilibrium equation with respect to the nodal out-of-plane displacement, whereas the functions h^- and h^+ are those of the same elements to the equilibrium with respect to the nodal rotation of the node i.

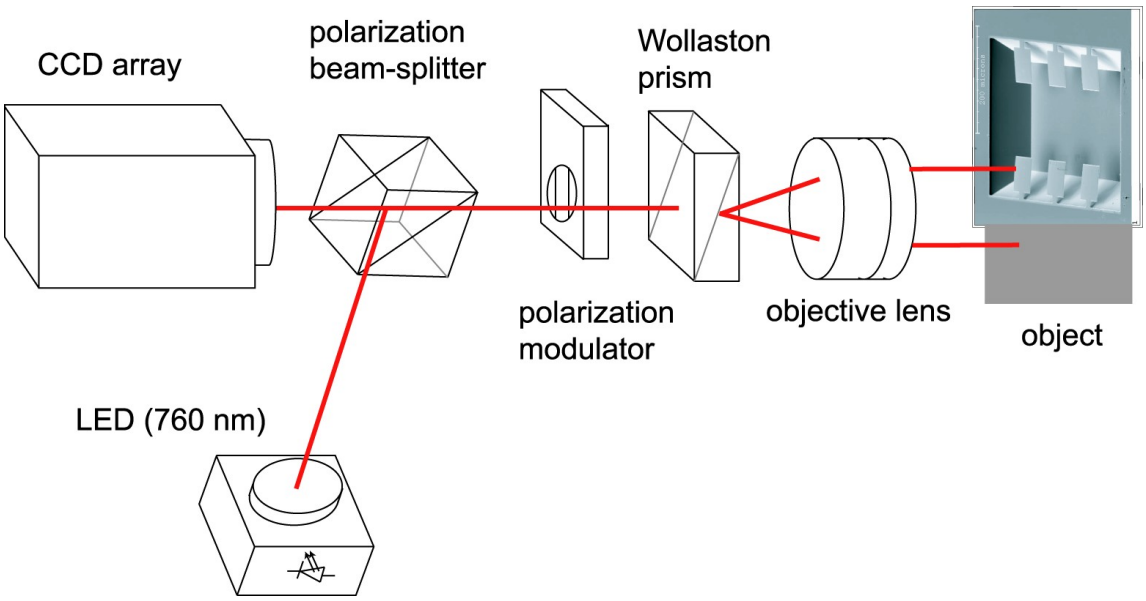

Figure 1. Description of the Nomarski shear-interferometer to measure out-of-plane displacement fields of MEMS.

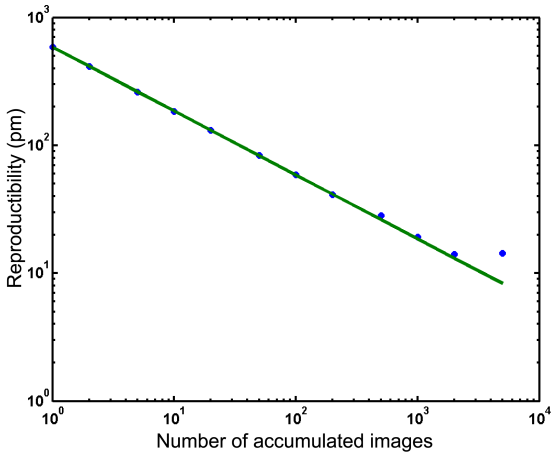

Figure 2. Estimation of the reproducibility on the measurement of a differential topography as a function of the number of accumulated images.

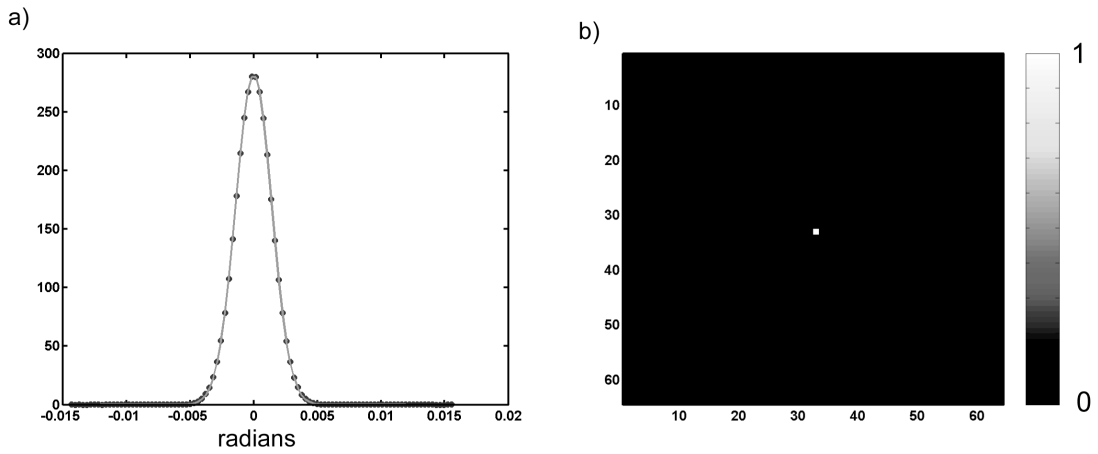

Figure 3. a) Experimental noise probability density (circles), and a zero-mean Gaussian distribution fit (solid line) b) Dimensionless autocorrelation function of a typical noise realization.

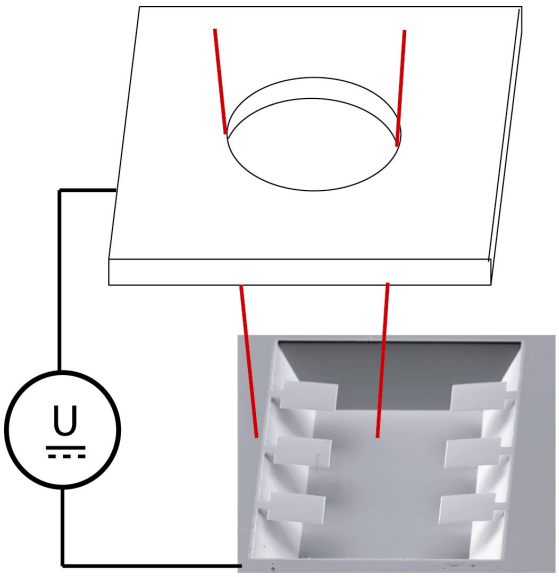

Figure 4. Schematic of the set-up used to apply an electrostatic pressure on a microcantilever.

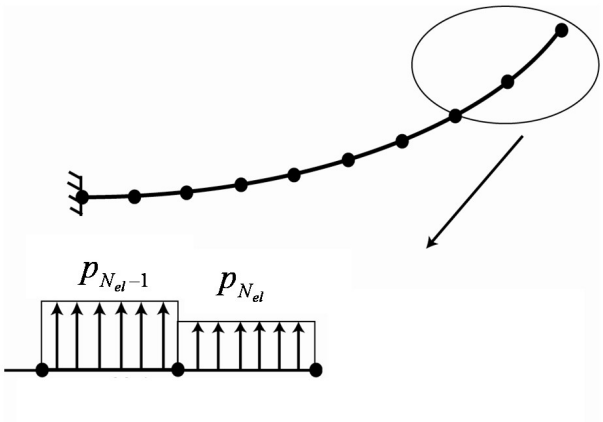

Figure 5. Description of the FE model.

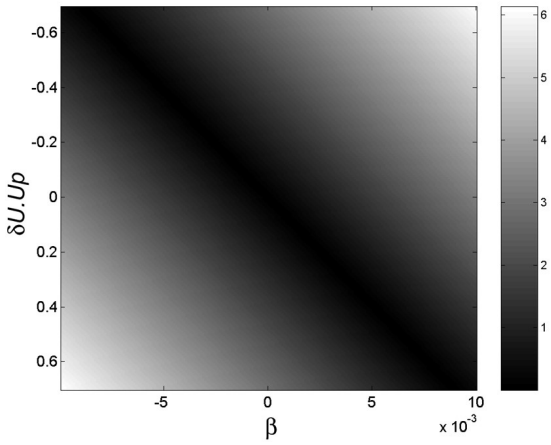

Figure 6. Norm of the residual in arbitrary units in the (β,δU^{t} . $U_{p.}$) plane.

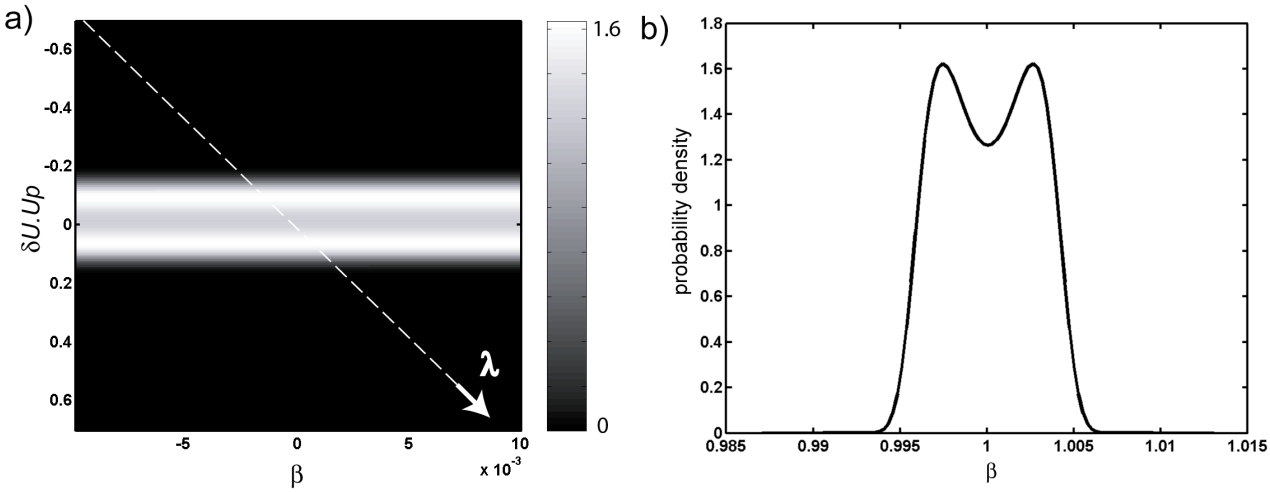

Figure 7. a) Probability density for κ in the (β,δU^t . $U_{p.}$) plane. b) Probability density for β.

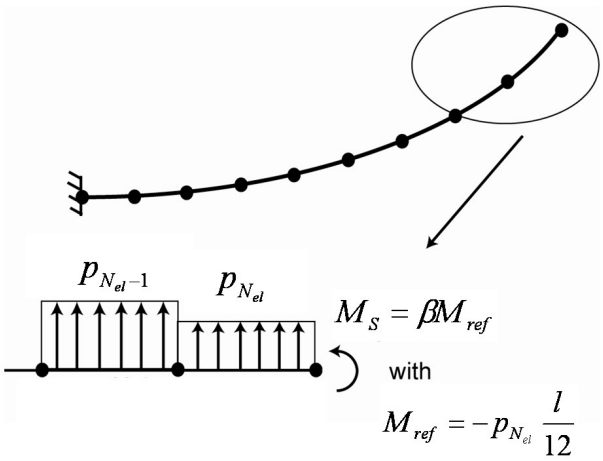

Figure 8. FE model for the experimental problem when an end couple is added.

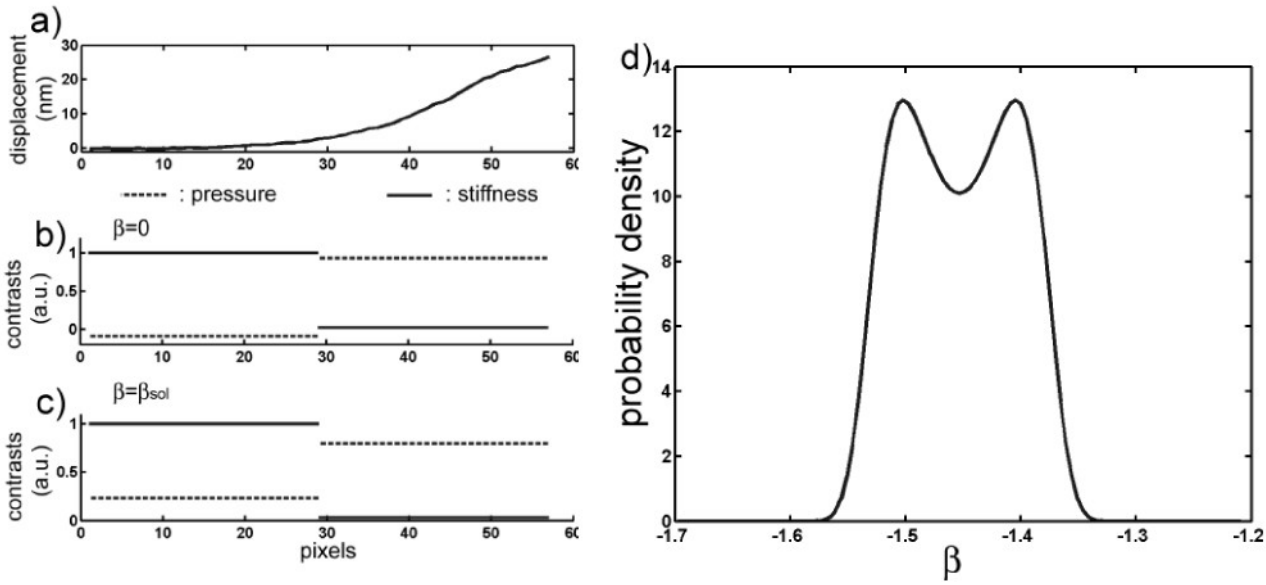

Figure 9. a) Measured displacement field b,c) Identified fields before and after accounting for a modeling error d) Probability density for β.